Replicating the Aerosol

S1-1 List of Experiments

Table S1-1. List of experiments performed and their chemical characteristics. Solution nomenclature is carried out through the supplemental information. Nuclear magnetic resonance (NMR) spectroscopy measurements were taken with 500 MHz 1H-NMR with 64 scans per measurement. $[BD]_0$ and $[NH_X]_0$ were determined from the mass of each species added to the mixtures. pH was estimated with in-situ quantitative measurements of the NMR shift of an acid.

Solution	Measurement	$[BD]_0$ (M)	$[NH_X]_0$ (M)	pH	Comment
BD_H2O_02	NMR	0.02	0	3[3]	Butenedial isomer analysis
BD_H2O_25	NMR	0.25	0	3[3]	Butenedial isomer analysis
BD_H2O_09	NMR	0.09	0	3[3]	Butenedial acetal formation
BD_H2O_55	NMR	0.55	0	3[3]	Butenedial acetal formation
BD_OH_pH8.8	NMR	0.2	0	8.8	R1 Fitting
BD_OH_pH9.5	NMR, MS[2]	0.2	0	9.5	R1 Fitting
BD_OH_pH9.8	NMR	0.2	0	9.8	R1 Fitting
BD_OH_pH10.4	NMR	0.2	0	10.4	R1 Fitting
BD_NH_pH3.6	NMR	0.4	0.4	3.6	Mechanism Validation
BD_NH_pH5	NMR, MS[1,2]	0.9	0.9	4.2-5.7	R2-R6 Fitting
BD_NH_pH8.5	NMR	0.9	0.2	8.5-8.8	Mechanism Validation

[1]The mass spectrometry (MS) spectra for BD_NH_pH5 was taken with a commercial time-of-flight mass spectrometer (JEOL AccuTOF) in positive ion mode only. [2]The MS spectra for BD_NH_pH5 and BD_OH_pH9.5 was taken with liquid chromatography – mass spectrometry in

positive and negative ion mode direct injection, respectively, coupled with UV/Vis absorption measurements spanning 300-450 nm. [3]These pH measurements were taken with litmus paper.

S1-2 Molecular Identification and Quantification

S1-2.1 Methodology

The solutions BD_NH_pH5 and BD_OH_pH9.5 were analyzed to identify reactants and products during reaction. Solutions with identical initial conditions were analyzed separately with MS and 1H-NMR, aside from the addition of internal standards added to solution to enable quantitation and pH estimation in the case of NMR.

High-resolution LC-MS measurements of each solution were recorded to identify the unambiguous molecular formula of major reaction products. Hexaethylene glycol (PEG-6) was added to BD_NH_pH5 as an internal standard for TOF-MS analysis. We did not identified interactions between butenedial and PEG-6 in a previous study (Birdsall et al., 2019). No internal standard was added to BD_OH_pH9.5 or BD_NH_pH5 for LC-MS analysis.

NMR was performed quantitatively using dilute (1-2% w/w) dimethyl sulfone (DMS) or diethylmalonic acid (DEM) as an internal standard, added to the solution. Concentrations of identified species were calculated with the relative signal intensity of their protons against that of DMS, as is described elsewhere (e.g., Yu et al., 2011). Areas of integration were estimated with MestReNova's line fitting software. The 1H-NMR spectra showed distinct groups of quantitative related signals that had similar temporal behavior. Each group of peaks whose quantitative signal strength behaved as integers and had the same temporal behavior was presumed to arise from a single compound. A molecular structure was proposed for each cluster of peaks and the molecular formulas mentioned above. In most cases, the quantitation was performed with a subset of the total peaks belonging to a molecule to avoid distortions from neighboring peaks and the background.

S1-2.2 Butenedial in H_2O

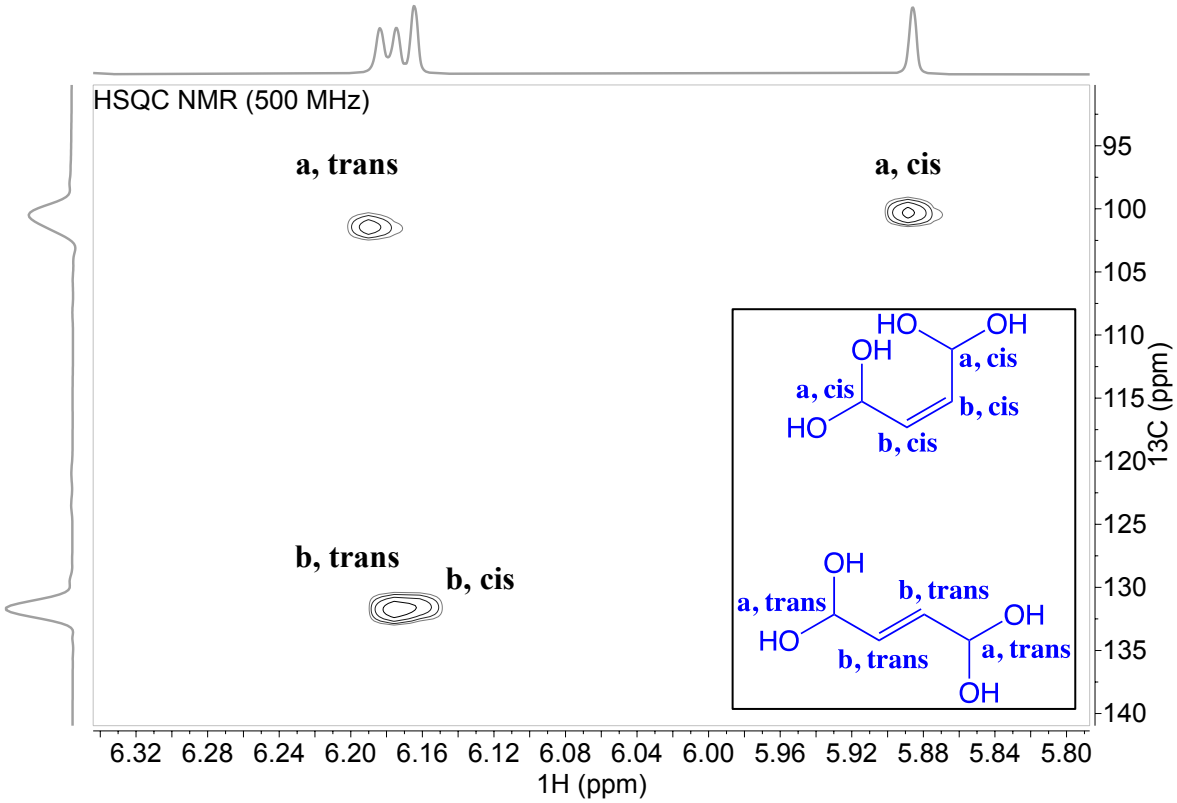

Figure S1-1. HSQC NMR spectrum of concentrated (~0.5 M) butenedial in D_2O. Butenedial (BD, $C_4H_8O_4$) is shown in the inset as a dihydrate, the dominant form of butenedial observed in aqueous solution, as both the cis and the trans isomer. The protons are assigned, according to their alphabetical labels, for both the cis and trans isomer. The proton with chemical shifts 6.17 and 5.86 ppm are assigned to the gem-diol carbon. The protons with chemical shifts 6.16 and 6.15 ppm are assigned to the alkene carbon. The upfield protons of each carbon are assigned to the cis isomer, and the downfield protons to the trans isomer, as is typical. Unhydrated BD was detected with MS at the m/z 85 channel.

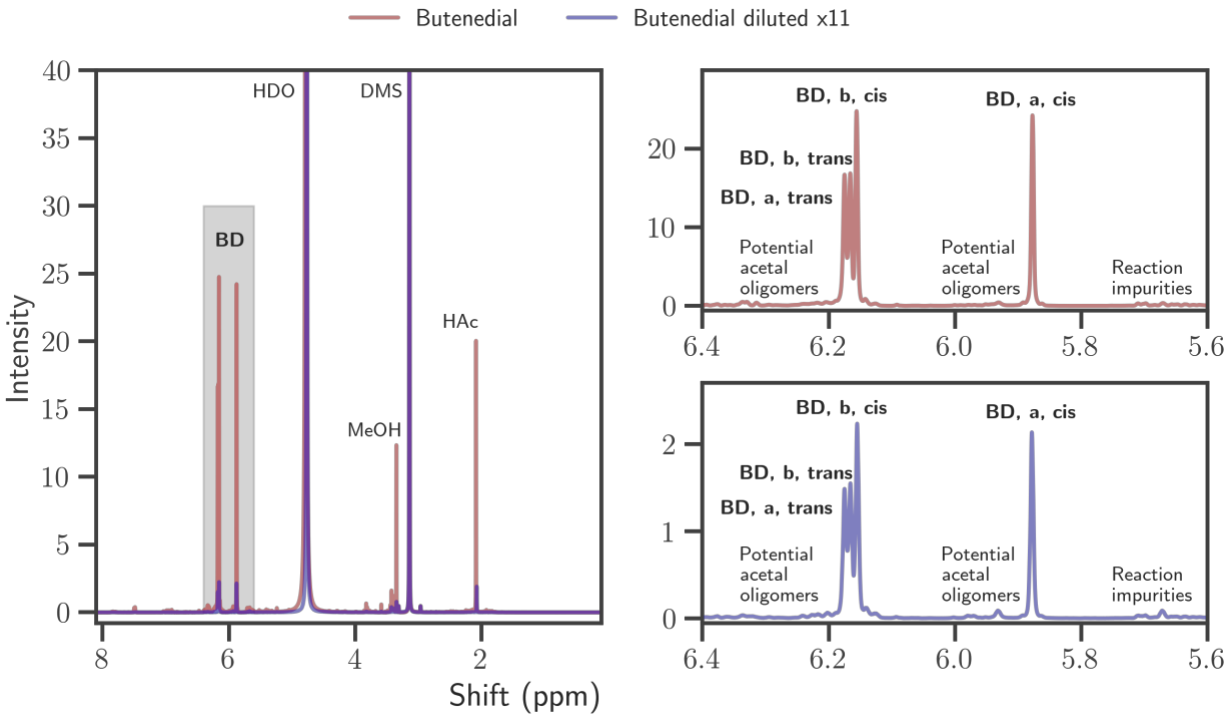

Figure S1-2. Species assignments in 1H-NMR spectra of the BD_H2O solutions, where one spectrum is taken of a solution (blue, BD_H2O_25) from an eleven-fold dilution of the other (red, BD_H2O_02). An overview spectrum is plotted to the left, and two expanded regions, identified by the shaded box, are plotted on the right for each of the spectra. Major peaks are labeled with their associated chemical compounds and corresponding protons (see Figure S1). The broad singlet at 4.76 is HDO (deuterium substituted water) solvent signal. Dimethyl sulfone (DMS) was the internal standard used as a reference and for quantitation. Acetic acid (HAc) is a nonreactive impurity from butenedial synthesis. Methanol (MeOH) is also detected as a nonreactive byproduct of the reaction.

Table S1-2. Reported quantitation of BD protons (see Figure S3) in BD_H2O solutions. Intensity (I) is reported assuming I(DMS) = 100. The ratio of cis to trans is near to unity.

Proton	Intensity (BD_H2O_25)	Intensity (BD_H2O_02)
BD, a, cis	25.8	2.8
BD, b, cis	25.0	2.6
BD, a, trans	20.0	2.4
BD, b, trans	25.0	2.2

Quantification of butenedial acetal oligomerization.

Table S1-3. Reported quantitation of BD_H2O_55 and BD_H2O_09 solutions. Three BD_H2O_55 solutions were each diluted approximately six-fold to BD_H2O_09 solutions,

according to the nominal dilution factor reported. The BD dihydrate molarities, measured in-situ, are provided as a comparison against the nominal dilution factor between pairs, to demonstrate if hydration speciation depends on BD concentration. The *maximum* BD acetal oligomer concentration is also presented, which was calculated by assigning the integrated signal intensity between 6.5-6.25 ppm and 6.15-5.9 ppm to a BD acetal dimer (with 8 assignable protons in this range). All values are given as averages and their standard deviations.

Solution	Measured [BD dihydrate]	Dilution factor	Measured max [BD acetal oligomer]
BD_H2O_55	0.55 ± 0.03 M	NA	0.023 ± 0.002 M
BD_H2O_09	0.089 ± 0.012 M	5.86 ± 0.12	0.003 ± 0.0005 M

Fratzke et al. (1985) define the equilibrium between monomer and hydrate dimer according to the following relation:

$$K = \frac{[D]}{[M]^2}$$

Where [D] is the hydrated dimer concentration and [M] is the monomer (hydrated or unhydrated) concentration. For glyoxal, K is reported to be 0.56 M^{-1} (Fratzke and Reilly, 1986). This results in a dimer concentration of 170 mM at a glyoxal monomer concentration of 0.55 M. Table S2 shows that the maximum butenedial acetal oligomer concentration can be at most 23 mM with 0.55 M butenedial dihydrate. This assumes that all signal specified in the caption to Table S2 corresponds to acetal oligomers and suggests that a tentative upper bound of the K estimate for butenedial is 0.08 M^{-1}. However, dilution experiments provide strong evidence that only a very small fraction of this signal corresponds to BD acetal oligomers:

If acetal dimers are formed, a dilution of butenedial solution leads to (1) a statistically significant decrease in butenedial concentration relative to the dilution factor and (2) a quadratic decrease in the dimer concentration compared to the butenedial monomer concentration.

1. The relative butenedial molarity of BD_H2O_55 to BD_H2O_09 is 6.28 ± 1.20 : 1 and the nominal dilution factor is 5.86 ± 0.12 (determined via the non-reactive standard). Thus, we do not find a significant difference between the nominal and measured concentration of butenedial dihydrate after dilution.
2. The decrease in maximum BD acetal oligomer concentration is 7.31 ± 1.43 from the dilution, which is far from quadratic with respect to the butenedial dihydrate decrease (which would be a factor of ~39). In addition, the upper limit of the observed BD acetal oligomer concentration post dilution, 0.0035M, is identical to the value calculated for the BD acetal oligomer concentration using upper limit of the dilution factor, 5.98, and the lower limit of the observed BD acetal oligomer concentration pre dilution, 0.021M. This indicates that the signal is predominantly from other compounds than acetal oligomers, which should equilibrate rapidly based on analysis of glyoxal acetal oligomers and general chemical considerations.

We therefore find that the presence of butenedial acetal oligomers is minimal, and clearly much less pronounced than for glyoxal.

S1-2.3 Butenedial + OH^- Reaction

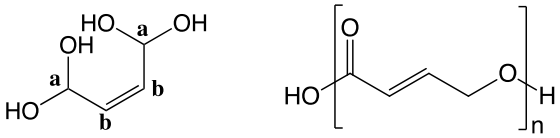

Butenedial (BD)

$C_4H_8O_4$
m/z 85

γ-hydroxycrotonic acid (GHC) oligomer

$[C_4H_4O_2]_n(H_2O)$
m/z 17 + 84n

Figure S1-3. Butenedial (BD) and γ-hydroxycrotonic acid (GHC) oligomer structures are shown in the figure above. GHC is an observed reaction product of the BD/OH^- reaction, which is analogous to other dicarbonyl disproportionation reactions, e.g., glyoxal to glycolic acid. GHC was not explicitly identified with NMR. The unit mass-to-charge (m/z) ratios of each species are given. BD dihydrate is the dominant form of BD observed in aqueous solutions. Unhydrated BD was detected with MS and the m/z ratio of its unhydrated forms is reported. The m/z ratios of protonated GHC are provided, although deprotonated GHC was detected with LC-MS, as shown in Figure S5 below.

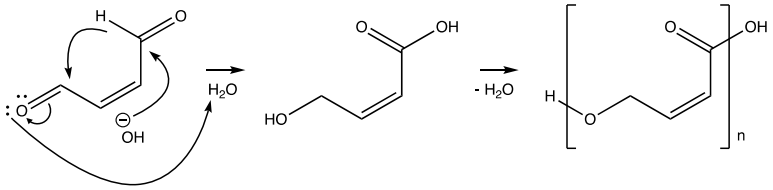

Figure S1-4. Proposed reaction scheme of hydroxycrotonic acid formation via OH^- substitution of butenedial and the Cannizzaro mechanism.

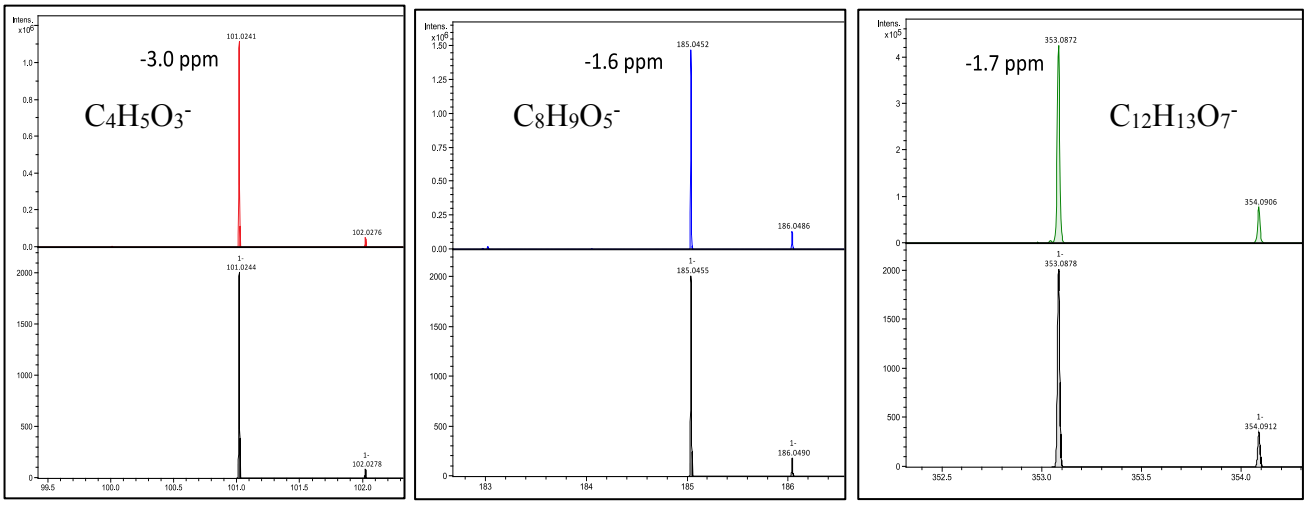

Figure S1-5. LC-MS (negative ion mode) taken of selected products observed in BD_OH_pH9.5 after approximately two hours of reaction. m/z channels 99-102 (left panel), 182-186 (middle

panel), and 352-354 (right panel) are shown as examples. The top row provides the observed mass spectrum and the bottom the theoretical isotopic pattern, which agree closely. Plots are not on equal scales. GHC monomer (m/z 101) dimer (m/z 185), and 4-mer (m/z 353) are observed from left to right. The exact mass is provided over the observed signal. The mass precision is provided in ppm left of the observed signal.

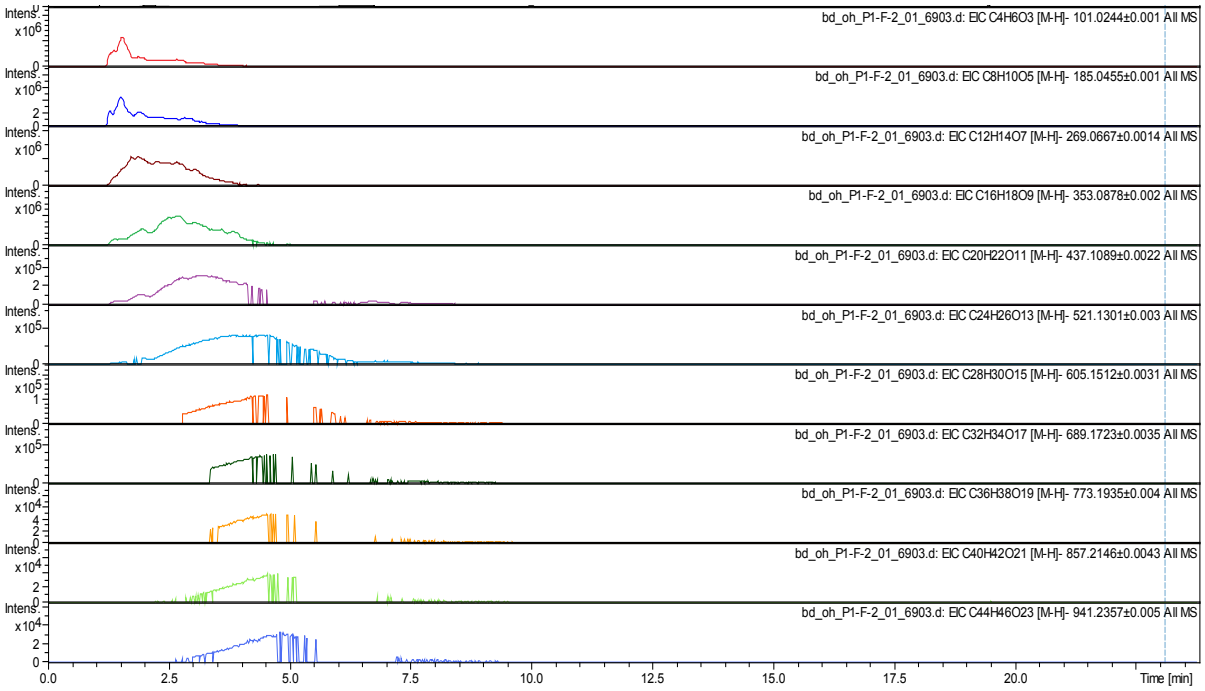

Figure S1-6. UV/Vis chromatogram spectra of selected products in BD_OH_pH9.5 samples observed with LC-MS, in negative ion mode. Spectra are plotted as light intensity as a function of time, and given for selected m/z channels. Absorbance of 300-450 nm light is observed for all selected n-mers (1-11) of hydroxycrotonic acid, sequentially from top panel to bottom panel.

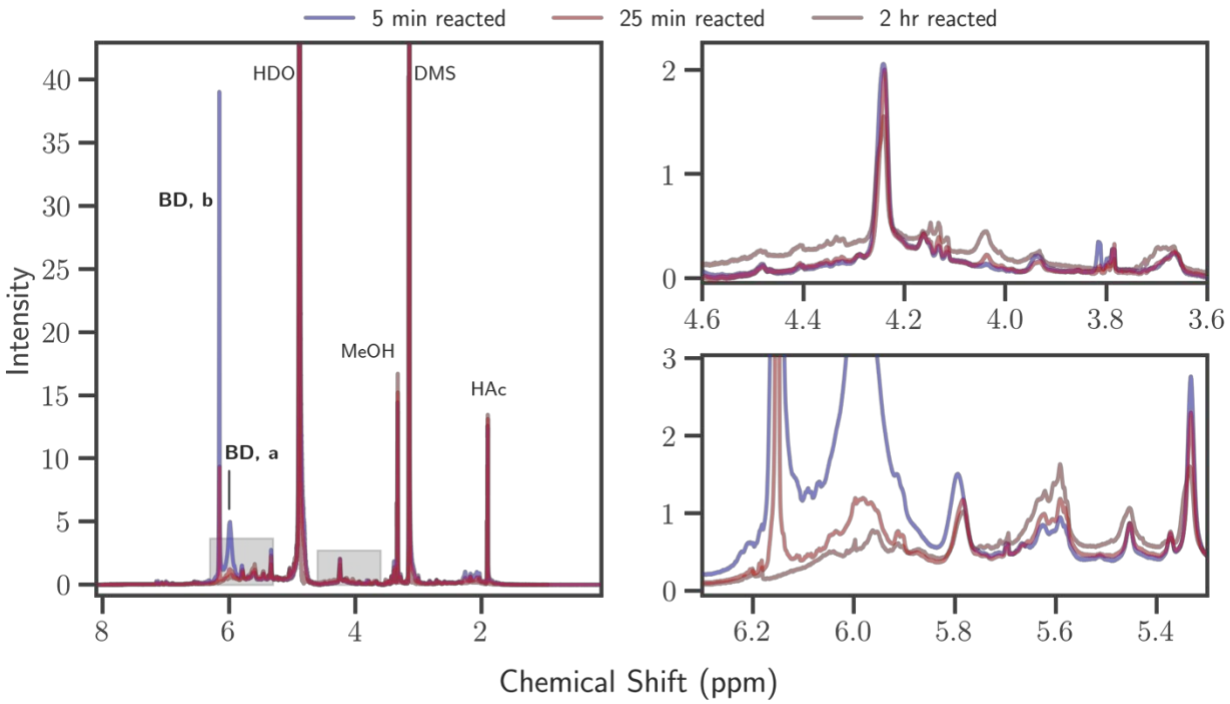

Figure S1-7. Product assignments in 1H-NMR spectra of the BD_OH solution, recorded 5 min (blue), 25 min (red), and 2 hr (brown) after mixing. An overview spectrum is plotted on top, and two expanded regions, identified by the shaded boxes, are plotted on bottom. Major peaks are labeled with their associated chemical compounds and corresponding protons (see Figure S3). The proton used for quantitation is identified with a bolded label. The butenedial gem diol protons are collapsed to one broad peak, as they may be exchanging with the solvent. The broad singlet at 4.76 is HDO (deuterium substituted water) solvent signal. Dimethyl sulfone (DMS) was the internal standard used as a reference and for quantitation. Acetic acid (HAc) is a nonreactive impurity from butenedial synthesis. Methanol (MeOH) is also detected as a nonreactive byproduct of the reaction. The buildup of the baseline at ~6.2-5 and ~4.5-3.6 ppm is expected to be from accretion reactions.

δ (ppm) of *butenedial dihydrate*: 6.15, 5.96

Notes on quantitation. For BD, the gem diol protons are less affected by the background than the alkene protons, and was therefore used in the quantitation, assuming a 2:1 gem diol to butenedial molar ratio.

Table S1-4. Reported quantitation of BD protons (see Figure S5) in BD_OH_pH10.4 solution at 5 min, 25 min, and 2 hr of reaction. Intensity (I) is reported assuming I(DMS) = 100. Intensities are insignificant of butenedial at 2 hr reaction. Near integer relationship between the two protons is observed.

Proton	Intensity (5 min)	Intensity (25 min)	Intensity (2 hr)
BD, a	0.425	0.141	0

BD, b	0.488	0.142	0

S1-2.4 Butenedial + NH_X Reaction

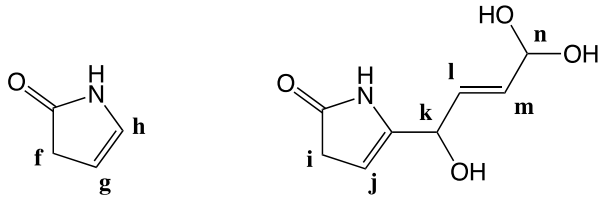

Pyrrolinone (PR)	**Butenedial-pyrrolinone dimer (BD-PR)**
C_4H_5ON	$C_8H_{11}O_4N$ ($C_8H_9O_3N$)
m/z 84	m/z 150 or 168

Figure S1-8. Pyrrolinone (PR) and butenedial-pyrrolinone dimer (BD-PR) structures are shown in the figure above. BD-PR hydrate is the dominant forms of BD-PR observed in aqueous solutions. Unhydrated BD-PR was detected with MS and the m/z ratio of its unhydrated forms is reported. PR and BD-PR are the major reaction products of the BD/NH_X reaction. The observed mass-to-charge (m/z) ratios of each species are given for adducts with H^+. The protons identified with NMR are labeled alphabetically for those attached to carbon atoms.

Butenedial/NH_X Reaction. We tentatively propose that butenedial/NH_X reaction proceeds as follows, although reaction intermediates are not observed with NMR or MS. Reaction begins when NH_3 attacks a protonated carbonyl carbon, forming an unstable hemiaminal that dehydrates to produce an imine. The imine can undergo ring closure, forming a hydroxypyrrole. The hydroxypyrrole is in equilibrium with pyrrolinone, which is the stable and favored form in an aqueous medium (Bocchi et al., 1970; Bordner and Rapoport, 1965; Hill et al., 2009). The ketonization of hydroxy heterocycles has been shown to increase with decreasing pH (Capon et al., 1987). As such, the tautomerization of pyrrolinone to the reactive hydroxypyrrole would be OH^--dependent. The proposed dimerization of butenedial with pyrrolinone takes place at the carbon adjacent to the NH group, as is typical for aldehyde/pyrrole reactions, e.g., in porphyrin synthesis (Koelsch and Richter, 1935).

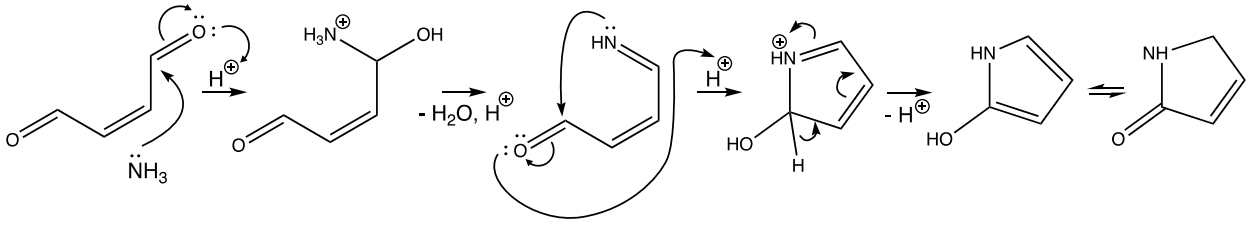

Figure S1-9. Pyrrolinone formation via NH_3 nucleophilic attack of butenedial, through Paul Knorr synthesis of pyrroles.

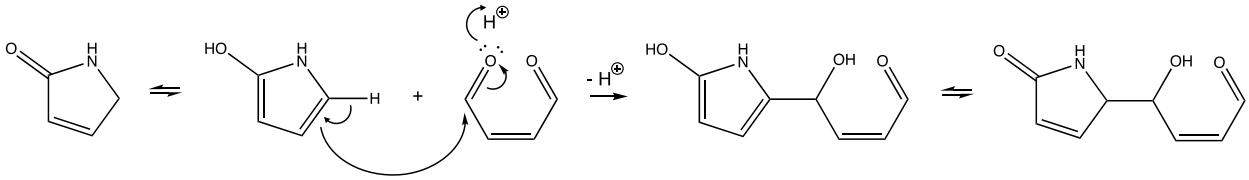

Figure S1-10. Butenedial-pyrrolinone "dimer" formation via butenedial electrophilic substitution reaction with pyrrolinone, analogous to porphyrin synthesis.

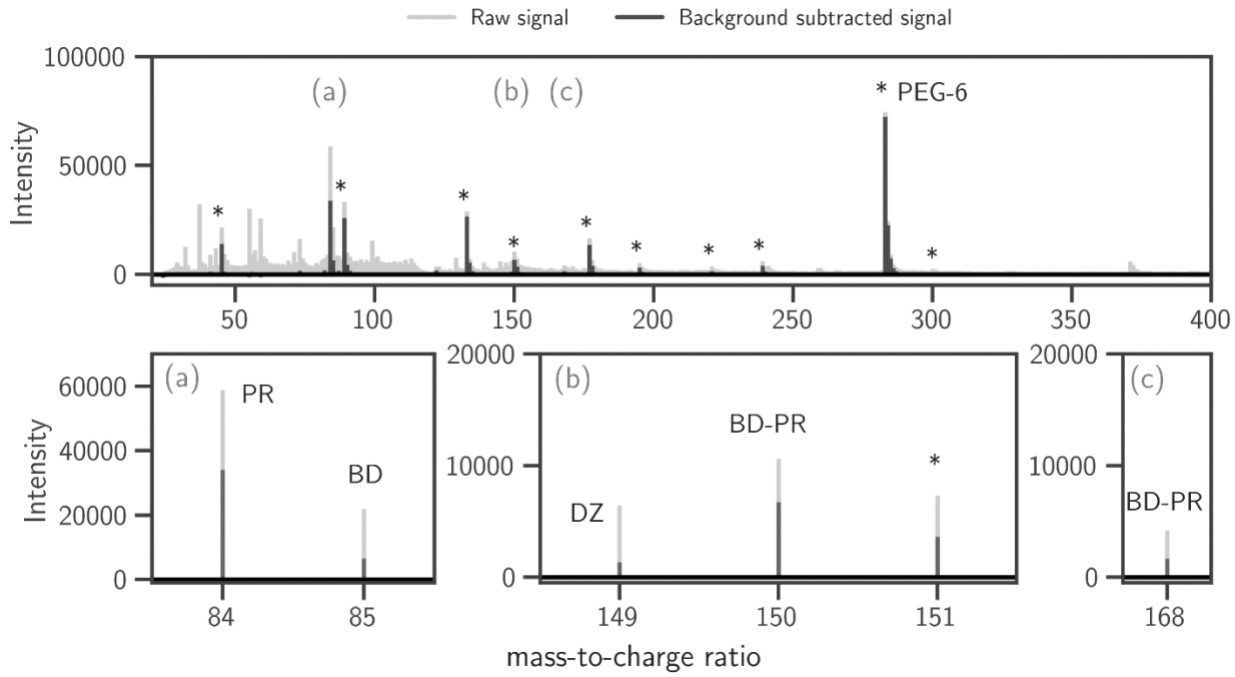

Figure S1-11. Spectrum of BD_NH_pH5 solution after ~20 minutes of reaction. Raw (gray) and background-subtracted (black) mass spectra are provided. The full spectrum is shown on the top panel, with lettered expanded regions on the bottom that demonstrate reactant and products. All species observed form adducts with H^+. Starred peaks correspond to PEG-6, its fragments, and clusters of water with PEG-6 and its fragments. These fragments were identified in previous studies (Birdsall et al., 2018, 2019). The background signal is residual from the experimental apparatus.

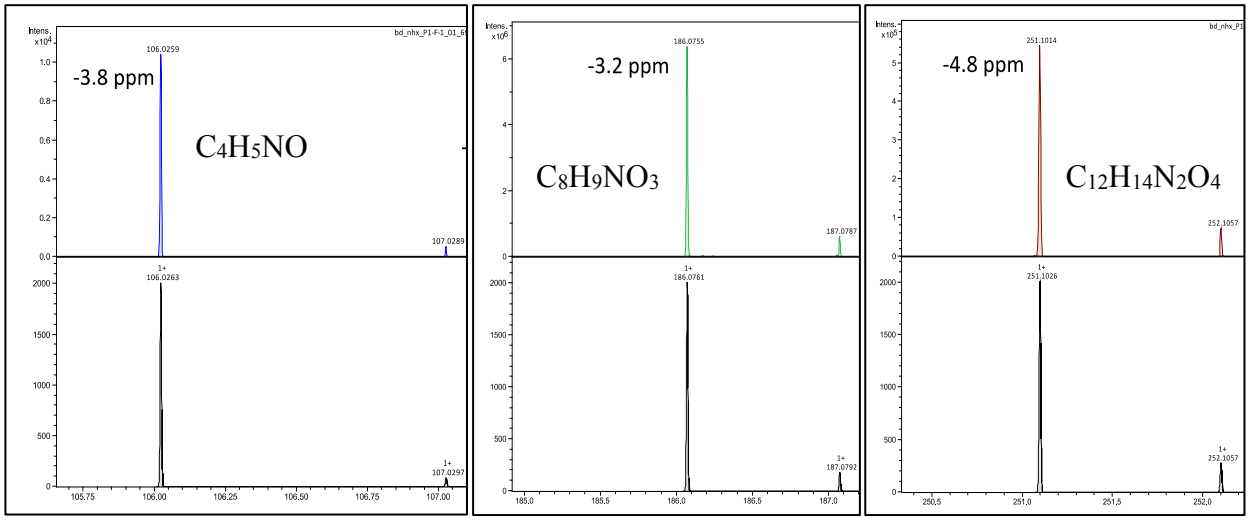

Figure S1-12. LC-MS (positive ion mode) taken of selected products observed in BD_NHx_pH5 after approximately two hours of reaction. m/z channels 106-107 (left panel), 185-187 (middle panel), and 250-252 (right panel) are shown as examples. The top row provides the observed mass spectrum and the bottom the theoretical isotopic pattern, which agree closely. Plots are not

on equal scales. Pyrrolinone (m/z 84), butenedial-pyrrolinone "dimer" (m/z 168), and a "trimer" from the addition of butenedial and NHx to the "dimer" (m/z 251) are observed from left to right. The exact mass is provided over the observed signal. The mass precision is provided in ppm left of the observed signal.

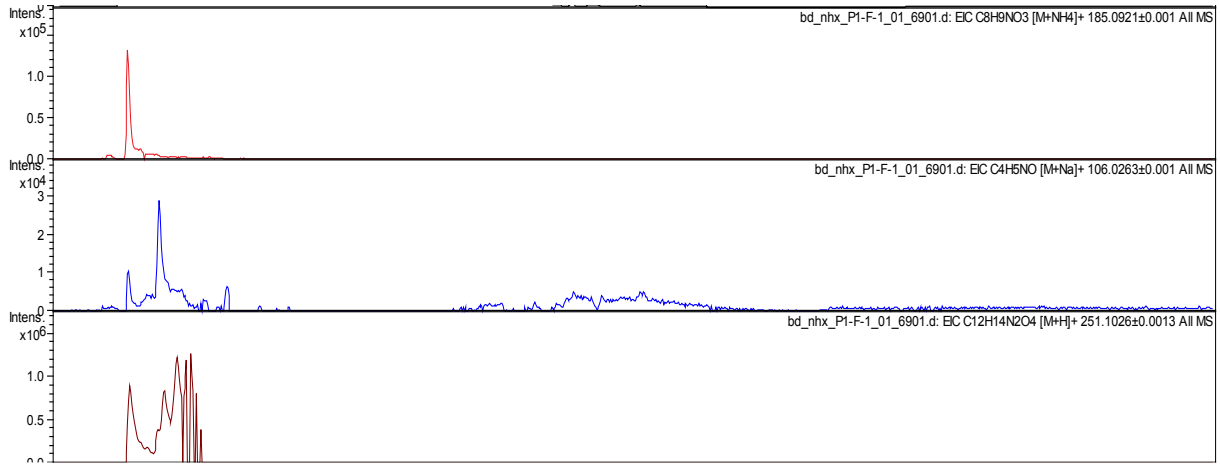

Figure S1-13. UV/Vis chromatogram spectra of selected products in BD_NHx _pH5 samples observed with LC-MS, in positive ion mode. Spectra are plotted as light intensity as a function of time, and given for selected m/z channels. Absorbance of 300-450 nm light is observed for butenedial-pyrrolinone "dimer," pyrrolinone, and a "trimer" ("dimer" with addition of butenedial and NHx), sequentially from top panel to bottom panel.

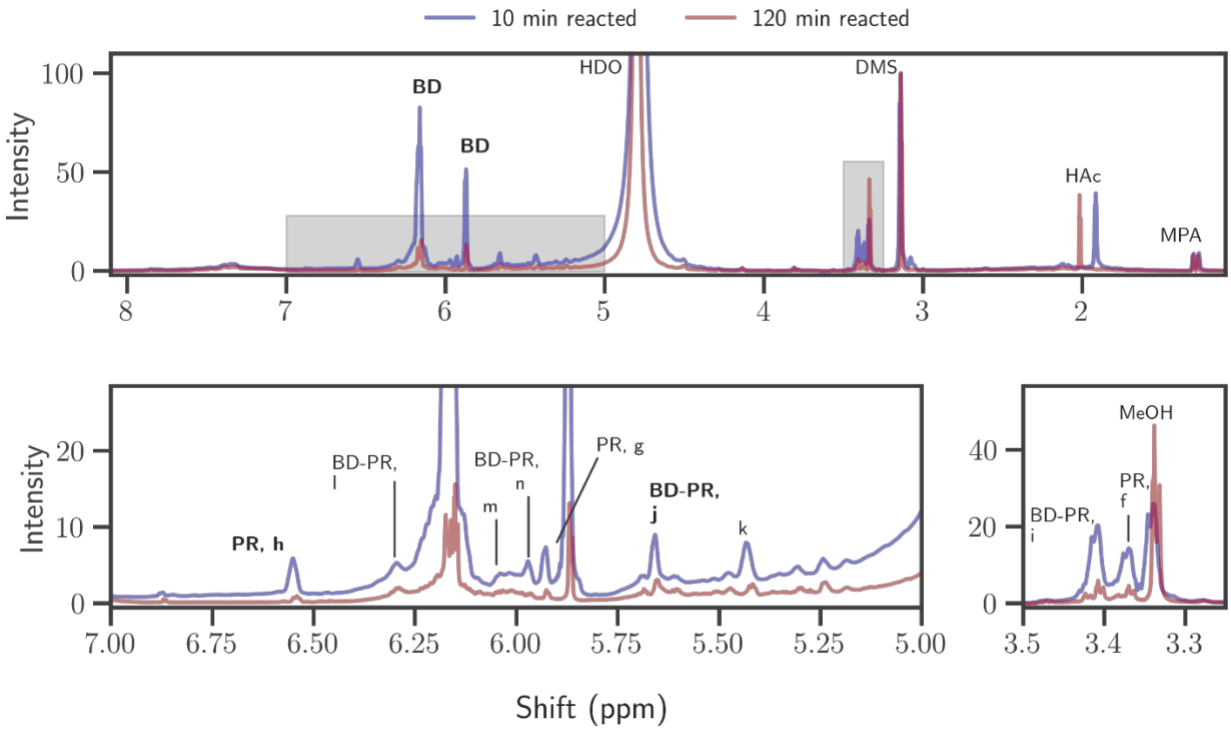

Figure S1-14. Proposed product assignments in 1H-NMR spectra of the BD_NH_pH5 solution, recorded after 10 min (blue) and 120 min (red) of reaction. An overview spectrum is plotted on top, and two expanded regions, identified by the shaded boxes, are plotted on bottom. Major peaks are labeled with their proposed associated chemical compounds and corresponding protons (see Figure S8). Asterisked labels indicate a proton in the cis or trans isomer. The proton used for quantitation is identified with a bolded label. The broad singlet at 4.76 is HDO (deuterium substituted water) solvent signal. Dimethyl sulfone (DMS) was the internal standard used as a reference and for quantitation. Methylphosphonic acid (MPA) was the internal standard used in conjunction with acetic acid (HAc), a nonreactive impurity from butenedial synthesis, for pH estimation. The change in HAc chemical shift observed between the two spectra is due to speciation changes from acid-base equilibrium. Methanol (MeOH) is also detected as a nonreactive byproduct of the reaction.

Proposed δ (ppm) of reactants and products. *Butenedial dihydrate*: 6.17, 6.16, 6.15, 5.86; *pyrrolinone*: 6.55, 5.92, 3.37; *butenedial-pyrrolinone dimer hydrate*: 6.29, 6.03, 5.97, 5.65, 5.43, 3.41.

Table S1-5. Reported quantitation of proposed BD, PR, and BD-PR protons (see Figure S8) in BD_NH_pH5 solution at 10 minutes and 120 minutes of reaction. Intensity (I) is reported assuming I(DMS) = 100. Intensity of protons from the cis and trans isomer are provided as tuples. In general, proximity to integer relationships is maintained across protons of a species through time. The NH proton was not used in quantitation.

Proton	Intensity (10 min)	Intensity (120 min)
BD, cis	69	14
BD, trans	56	11
PR, f	18	3.7
PR, g	7.4	2.0
PR, h	11	2.0
BD-PR, i	32	9.0
BD-PR, j	14	4.0
BD-PR, k	12	4.3
BD-PR, l	12	4.0
BD-PR, m	10	N/A[1]
BD-PR, n	12	N/A[1]

[1]The signal of these proposed protons of BD-PR was not resolved with the integration software at 120 minutes, presumably due to overlapping signal.

Notes on quantitation. For BD, the total proton signal was used to perform the quantitation when the BD signal was sufficiently higher than the background, approximately 10 intensity units. The upfield gem-diol proton (a, cis) is less affected by the background than the other protons, and it is observed that the ratio of cis to trans (~0.55/0.45) is constant during reaction. At low BD signal intensity, the BD quantitation was performed by multiplying the upfield gem-diol proton

(a, cis) signal by 1.8 to obtain total butenedial concentration, both cis and trans forms. PR quantitation was performed with the downfield alkene proton (h). BD-PR quantitation was performed with the heterocyclic alkene proton (j).

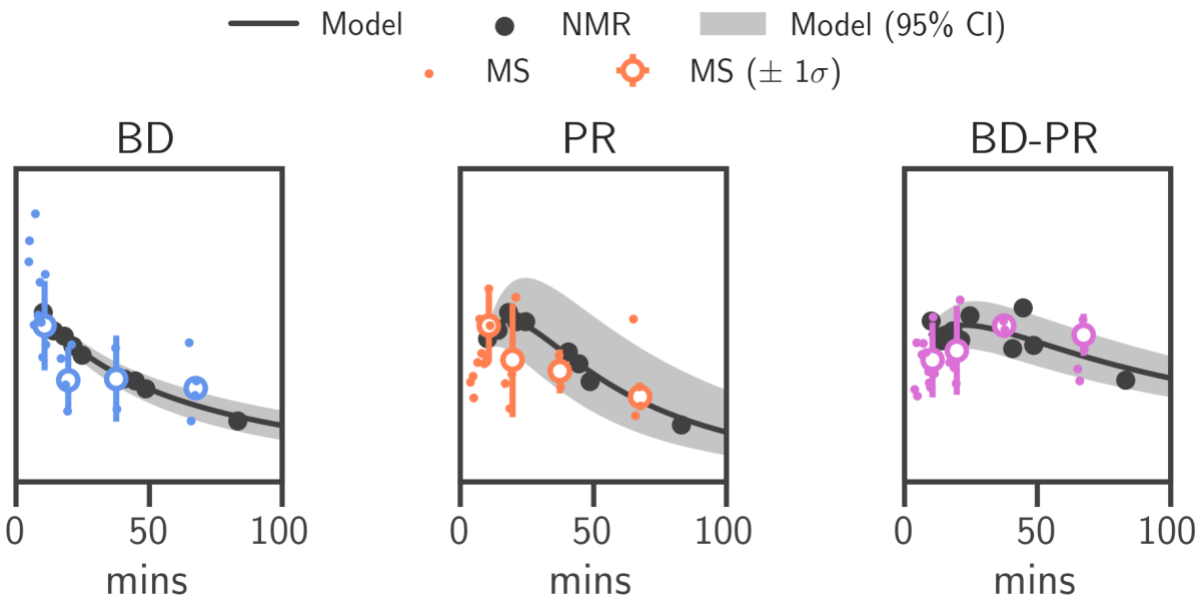

Figure S1-15. Comparison of MS and NMR measurements of butenedial, pyrrolinone, and butenedial-pyrrolinone "dimer" (left to right) in equivalent BD_NHx_pH5 reaction mixtures, in arbitrary units. MS measurements are signal of analyte normalized to hexaethylene glycol signal, used as an internal standard that is nonreactive toward butenedial, NMR are reported as concentrations. The kinetic model mechanism output, equivalent to that shown in Figure 3 of the main text is overlaid over each panel.

S1-2.5 Images of aqueous solutions during reaction

Figure S1-16. BD_OH_pH8.8 (left) and BD_OH_pH10.4 (right) solutions in an NMR tube after ~40 minutes of reaction. A color change was immediate. No solids were observed in BD_OH_pH8.8, BD_OH_pH9.5, BD_OH_pH9.8, or BD_OH_pH10.4 solutions.

Figure S1-17. Series of 0.4 M BD/0.2 M AS solutions at increasing time of reaction rightward (left). 0.4 M BD/0.2 M AS solution after weeks of reaction (right). Solutions had approximately the same starting composition. The solutions darken over time and solids appear to form. A visible color change to a darker yellow was observed within minutes. Black-brown color was noticeable after hours of reaction. The accumulation of solids occurred on longer timescales (many hours to days). Solids were also observed rapidly (under an hour) in BD/NH_X solutions with higher pH (e.g., in BD_NH_pH8.5 experiments).

S1-3 Parametrizations

S1-3.1 pH estimation with NMR

pH estimation with 1H-NMR is described elsewhere in detail (Wallace et al., 2018). In brief, dilute (<1% w/w) acid is added to solution, and selected such that its pKa ~ solution pH ± 2. Acetic acid is present as an impurity in the starting material and is also used as a pH indicator. The acids used are described in Table S5. pH is calculated from the recorded chemical shift (δ) of the acid via the equation below, where δ_{A-} and δ_{HA} are the chemical shifts of the deprotonated and protonated acid, respectively. δ_{A-} and δ_{HA} were recorded in this study and closely match those reported by Wallace et al. (2018).

$$pH = pKa + log_{10}\left(\frac{\delta_{A-} - \delta}{\delta_{A-} - \delta_{HA}}\right)$$

Table S1-6. pH indicator, relevant quantities, and use in experimental runs of this work.

Indicator	pKa	δ_{A-}	δ_{HA}	Experiments used
Acetic acid	4.58[1]	1.90	2.09	BD_NH_pH5, BD_NH_pH3.6
Methylphosphonic acid	7.78[1]	1.07	1.29	BD_OH_pH8.8, BD_OH_pH9.5, BD_NH_pH8.5
2,4,6-trimethylphenol	10.88[2]	6.36	6.62	BD_OH_pH9.8, BD_OH_pH10.4

[1]Values given by Wallace et al. (2018). [2] Retrieved from: National Center for Biotechnology Information. PubChem Compound Summary for CID 10698, 2,4,6-Trimethylphenol. https://pubchem.ncbi.nlm.nih.gov/compound/2_4_6-Trimethylphenol. Accessed Feb. 9, 2021.

S1-3.2 Butenedial/OH^- rate constant (k_1) vs. pH

The fitting of the rate constant k_1 as a function of pH is shown in Figure S11 below. As mentioned in Section 2, at constant pH, the reaction of dialdehydes with OH^- is an apparent first order rate law that is linearly dependent on the dialdehyde. In each experiment, pH was held constant with a carbonate buffer system and monitored with NMR. The decay of butenedial in four experiments at different pH was measured and a first-order linear fit was applied using Python's scipy package. Specifically, the lmfit library with the Levenberg-Marquardt algorithm was used to perform the least squares minimization. A Monte Carlo simulation was performed to derive the reported 95% confidence intervals on model runs. The extracted k_1 values from the model fit, reported for each experiment in Figure S11 below, were used to fit the empirical formulation, demonstrated in Section 3.2 of the main text.

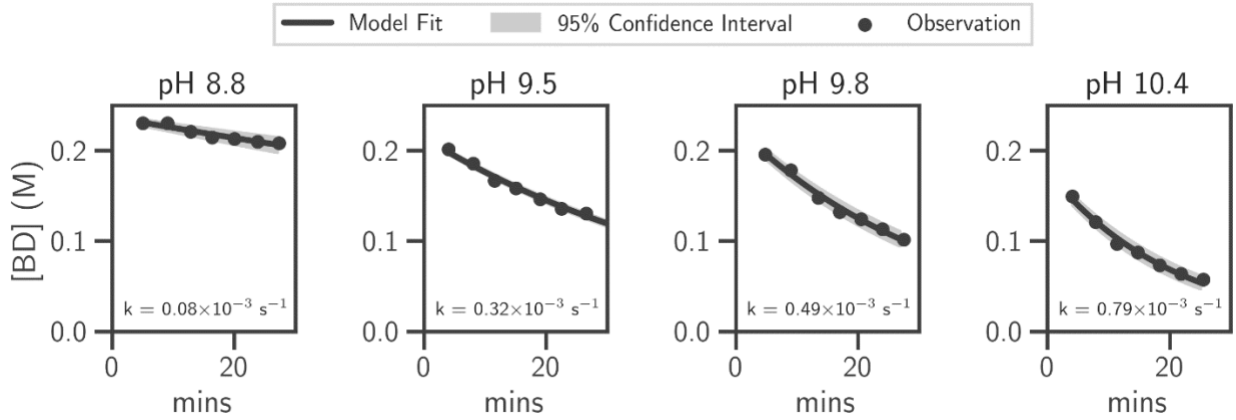

Figure S1-18. The loss of butenedial due to disproportionation reaction with OH^- is shown for four experiments at different pH. The pH was held constant and is shown above each panel. Measurements were performed with 1H-NMR. Modeled fits were performed with a linear regression of the natural logarithm of the concentration data. First-order rate constants (i.e., k_1) were extracted from the modeled fits and are shown on each panel. 95% confidence interval of the fitting is shown.

S1-3.3 pH empirical fit

Experimental pH was observed to closely follow a curve of the form

$$pH(t) = \frac{a\ t}{b\ t + c}$$

in BD_NH_pH5 and BD_NH_pH8.5 observations. pH decrease is observed in glyoxal/NH_X reactions as well (Yu et al., 2011).

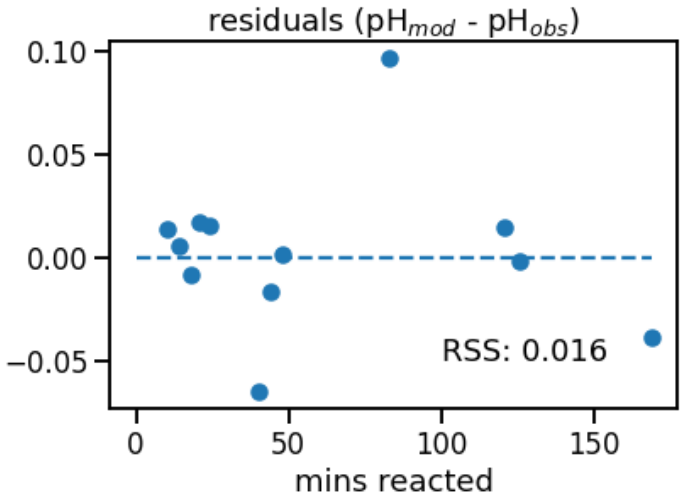

Figure S1-19. Residuals of median estimated and observed pH in BD_NH_pH5 measurements are shown below. There is not a clear trend in the residuals, which are all within 0.1 pH units.

S1-3.3 Sensitivity of kinetic mechanism to NH_X estimation

As explained in Section 2 of the main text, NH_X was not explicitly measured and instead estimated through a 1:1 loss rate with butenedial (i.e., per butenedial lost, one NH_X is lost). This assumption will overestimate NH_X loss when butenedial is consumed by accretion reactions that do not additionally consume NH_X. The sensitivity of the mechanism to the NH_X estimation technique is assessed by comparing the parametrization against the other extreme scenario: constant NH_X, i.e., $NH_X(t) = NH_{X,0}$. The difference in the parameter estimates is a measure of the maximum attainable variability between NH_X estimation techniques.

$$S_i = \frac{|k_{i,0} - k_{i,1:1}|}{k_{i,1:1}}$$

The sensitivity (S) is calculated by taking the difference between parameter estimates from the constant NH_X (subscript 0) and 1:1 butenedial and NH_X loss (subscript 1:1) scenarios, relative to the estimate recorded for the 1:1 loss scenario. For example, a value of 1 indicates that difference in estimates is equal to the estimate. The estimates are taken from model fits to BD_NH_pH5 data.

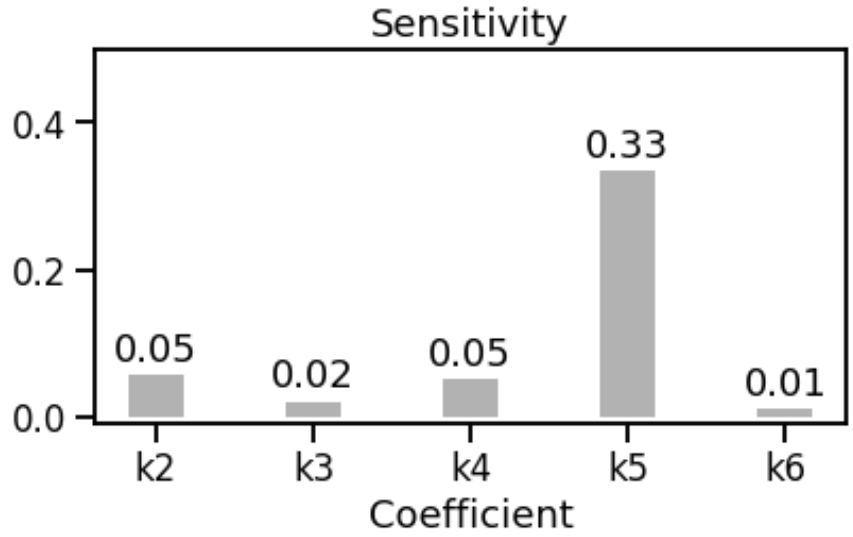

Figure S1-20. Sensitivities of the parameter estimates to NH_X estimation technique (1:1 NH_X:butenedial removal or constant NH_X). Most sensitivities are <0.05 the parameter estimate, indicating that those parameters (k_2, k_3, k_4, k_6) are not affected significantly by the NH_X estimation technique. k_5, i.e., removal of pyrrolinone through accretion reactions, is much more sensitive to the estimation technique. This may indicate that the pyrrolinone removal term is the least constrained of the parameters.

S1-3.4 Assessment of reaction mechanism

The kinetic mechanism described in DE1-3 and Table 3 in the main text is evaluated through comparisons against measurements of butenedial taken from different experiments (BD_NH_pH3.6 and BD_NH_pH8.5). The pH and initial conditions of the experiments, described in Table S1, were taken as model inputs. Model outputs and experimental measurements of butenedial are shown in Figures S14 and S15 and generally indicate that the kinetic mechanism can predict butenedial loss in aqueous solutions containing ammonia at a range of pHs.

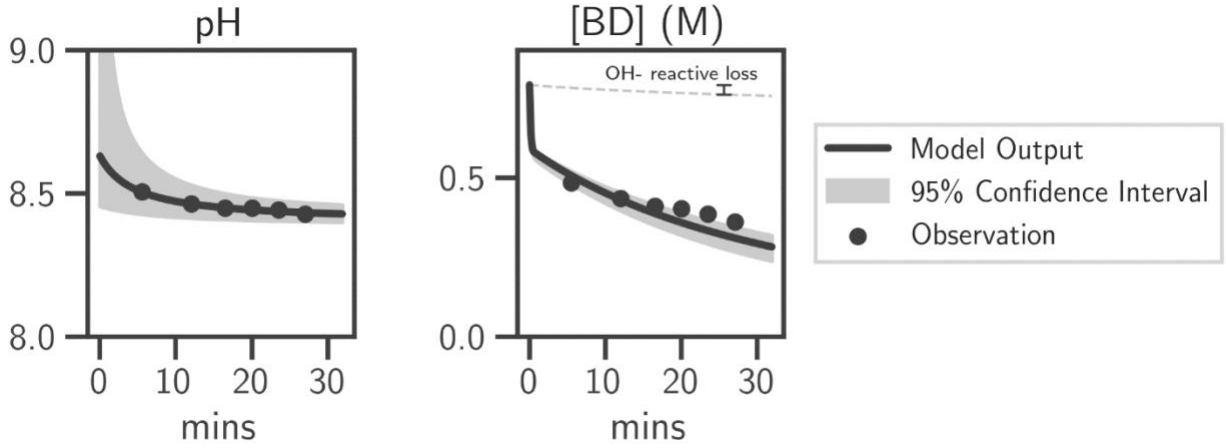

Figure S1-21. Experimental observations of BD_NH_pH8.5 against model outputs of the kinetic mechanism taken with the recorded pH and same initial conditions. pH was modeled with an empirical fit described in Equation. The initial pH conditions are poorly constrained by the empirical fit, although the median agrees with a starting pH of >8-9 witnessed with litmus paper. Butenedial is removed rapidly until all NH_X is consumed. The remaining butenedial decays at a slower pace through accretion reactions. Loss due to reaction with OH^- is shown to be a minor sink of butenedial at pH 8.5 compared to loss from reaction with NH_X and accretion reactions.

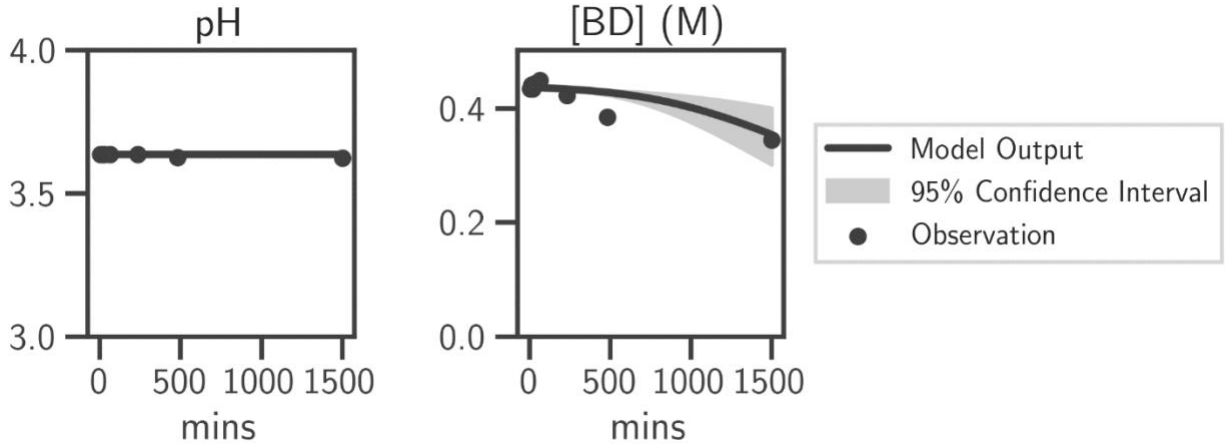

Figure S1-22. Experimental observations of BD_NH_pH3.6 against model outputs of the kinetic mechanism taken with the recorded pH and same initial conditions. pH was approximately

constant throughout the experimental run. Modeled butenedial agrees with butenedial measurements generally, with the exception of a slight overestimation compared to the measurement taken at ~500 minutes of reaction.

S1-4 References

Bader, R. F. W.: Atoms in molecules : a quantum theory, Clarendon Press, Oxford., 1990.

Birdsall, A. W., Krieger, U. K. and Keutsch, F. N.: Electrodynamic balance–mass spectrometry of single particles as a new platform for atmospheric chemistry research, Atmos. Meas. Tech., 11(1), 33–47, https://doi.org/10.5194/amt-11-33-2018, 2018.

Birdsall, A. W., Hensley, J. C., Kotowitz, P. S., Huisman, A. J. and Keutsch, F. N.: Single-particle experiments measuring humidity and inorganic salt effects on gas-particle partitioning of butenedial, Atmos. Chem. Phys., 19(22), 14195–14209, https://doi.org/10.5194/acp-19-14195-2019, 2019.

Bocchi, V., Chierici, L., Gardini, G. P. and Mondelli, R.: On pyrrole oxidation with hydrogen peroxide, Tetrahedron, 26(17), 4073–4082, https://doi.org/10.1016/S0040-4020(01)93048-0, 1970.

Bordner, J. and Rapoport, H.: Synthesis of 2,2'-Bipyrroles from 2-Pyrrolinones [1a], J. Org. Chem., 30(11), 3824–3828, https://doi.org/10.1021/jo01022a053, 1965.

Capon, B., Guo, B.-Z., Kwok, F.-C. and Wu, Z.-P.: Some studies on the tautomerism of heterocyclic and homocyclic compounds, Pure and Applied Chemistry, 59(12), 1577–1584, https://doi.org/10.1351/pac198759121577, 1987.

Fratzke, A. R. and Reilly, P. J.: Thermodynamic and kinetic analysis of the dimerization of aqueous glyoxal, Int. J. Chem. Kinet., 18(7), 775–789, https://doi.org/10.1002/kin.550180705, 1986.

Hill, L., Imam, S., McNab, H. and O'Neill, W.: 3-Hydroxy-1H-pyrrole, Synthesis, 2009(15), 2535–2538, https://doi.org/10.1055/s-0029-1217422, 2009.

Wallace, M., Adams, D. J. and Iggo, J. A.: Titrations without the Additions: The Efficient Determination of p K_a Values Using NMR Imaging Techniques, Anal. Chem., 90(6), 4160–4166, https://doi.org/10.1021/acs.analchem.8b00181, 2018.

Yu, G., Bayer, A. R., Galloway, M. M., Korshavn, K. J., Fry, C. G. and Keutsch, F. N.: Glyoxal in Aqueous Ammonium Sulfate Solutions: Products, Kinetics and Hydration Effects, Environ. Sci. Technol., 45(15), 6336–6342, https://doi.org/10.1021/es200989n, 2011.

S2-1 List of experiments

Table S2-1. Experiments performed in this study, which are referred to throughout the supplemental material. Concentrations of butenedial (BD), reduced nitrogen (NH_X), sulfate (S(VI)), hexaethylene glyoxal (PEG-6), and water mole fraction (X_{H2O}) were estimated with the relative humidity (~75%) and AIOMFAC, as described in the main text. Measurements were taken with mass spectrometry (MS) or nuclear magnetic resonance (NMR) spectroscopy. The NH_3 mixing ratio (C_{NH3}) was estimated with the equilibrium partitioning of ammonia (NH_3) between droplet and purge gas, as is described in the main text.

Experiment	$[BD]_0$ (M)	$[NH_X]_0$ (M)	[S(VI)] (M)	[PEG-6] (M)	X_{H2O}	C_{NH3} (ppm)
Butenedial/AS bulk liquid (MS)	0.4	0.4	0.2	0.7	0.95	0
Butenedial/AS bulk liquid (MS)	0.9	0.9	0.45	0.35	0.92	0
Butenedial/AS bulk liquid (NMR)	0.9	0.9	0.45	0	0.93[a]	0
Butenedial/AS particle (MS)	1.0	1.0	0.5	1.8	0.80	0
Butenedial particle (MS)	1.6	0	0	1.9	0.80	0
Butenedial/SS particle (MS)	1.6	0	1.8	0.9	0.80	0
Butenedial particle + NH_3(g) (MS)	1.6	0	0	1.4, 1.9[b]	0.80	0.7, 3.5, 18, 180

[a]D_2O was the primary solvent. Additionally, <1 % w/w dimethyl sulfone and methyl phosphonic acid were added as internal standards, as is described by Hensley et al.[1] [b]PEG-6 concentration was 1.4 M in the 0.7 ppm NH_3 experimental run and 1.9 M in the 3.5, 18, and 180 ppm NH_3 experimental runs.

S2-2 Mass spectrometry data

S-2.1 Sample measurements with mass spectrometry

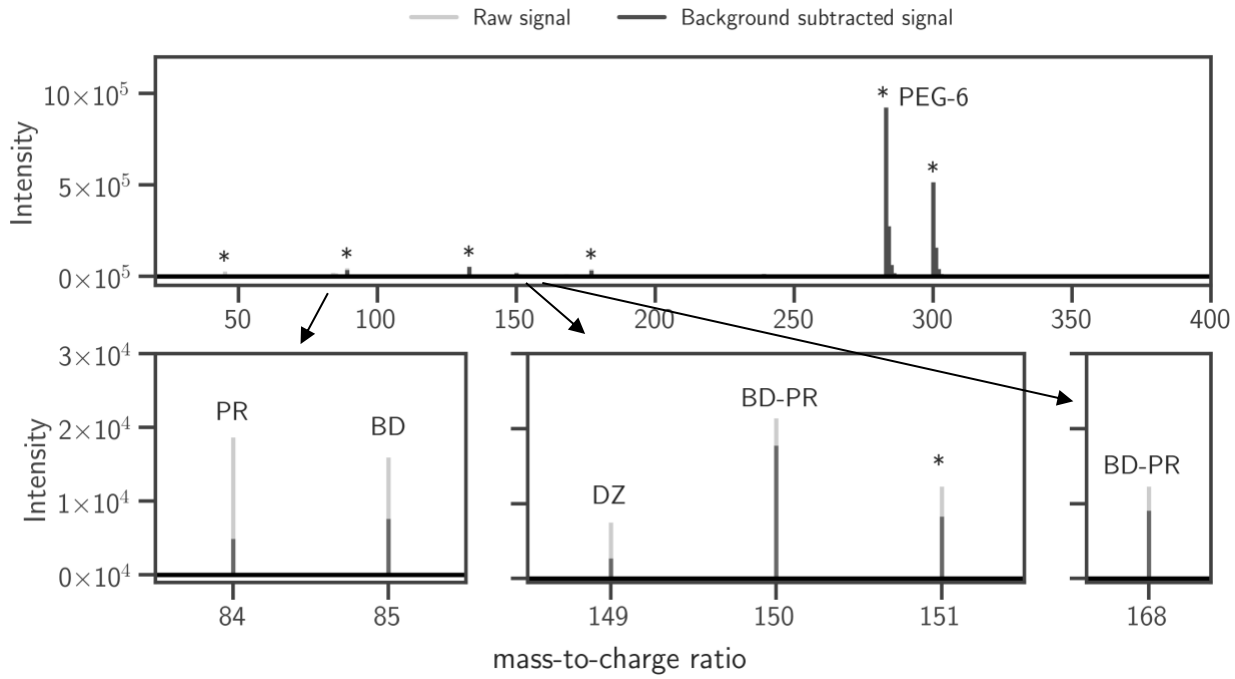

Figure S2-1. Sample mass spectrum taken of a particle levitated for ~15 minutes exposed to 3.5 ppm NH_3. Raw (gray) and background-subtracted (black) mass spectra are provided. The full spectrum is shown in the top panel, with lettered expanded regions on the bottom that demonstrate reactant and products. All species observed form adducts with H^+. Diazepine (DZ, m/z 149) is a minor product and is not considered in the kinetic and chemical analysis.[1] Starred peaks correspond to PEG-6 (m/z 283), its fragments, clusters of water with PEG-6 and its fragments, and PEG-6 adduct with NH_4^+ (m/z 300). These fragments were identified in previous studies.[2,3] The background signal is residual from the experimental apparatus.

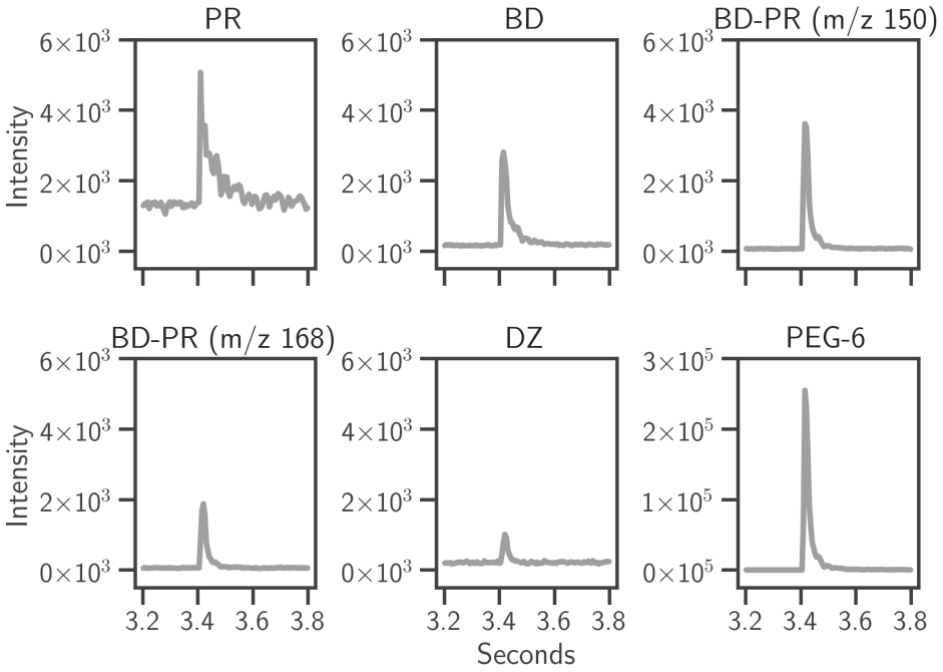

Figure S2-2. Sample extracted ion time series from measurement of a single particle, with mass spectrum shown in Figure S2. The peak intensities in each of the species mass channels above the surrounding background are used to quantify their abundance. The PEG-6 ion time series is taken of the parent ion at m/z 283.

S2-2.2 BD-PR mass-to-charge channel

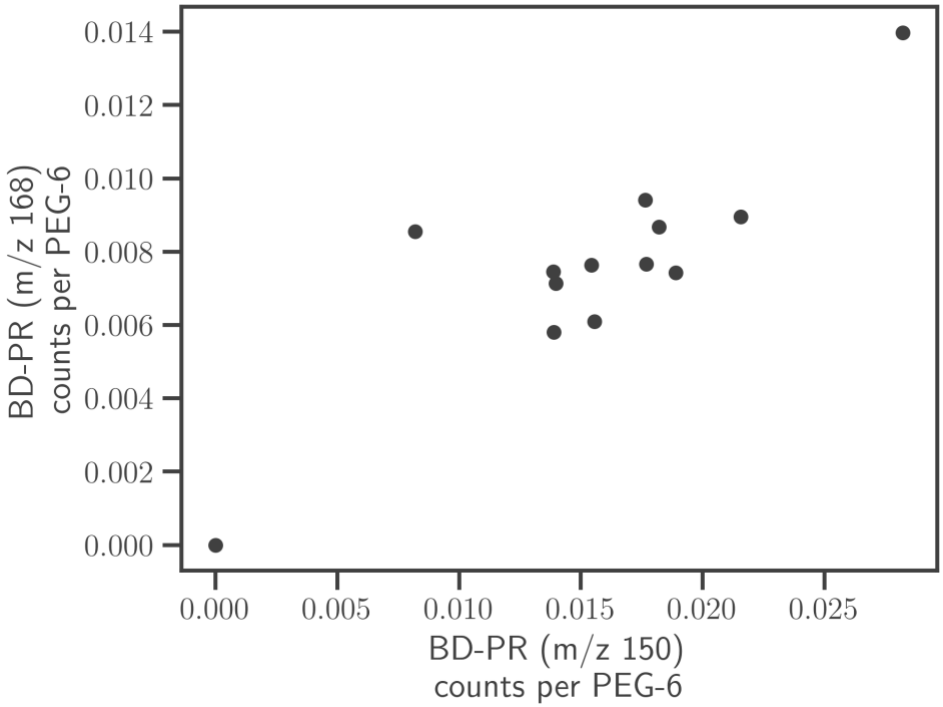

Figure S2-3. Comparison of measurements of butenedial-pyrrolinone dimer taken at two mass-to-charge channels, m/z 150 and m/z 168 in butenedial levitated particles exposed to 3.5 ppm NH_3. The m/z 150 channel is used in all analyses due to the higher sensitivity of BD-PR dimer at this channel.

S2-2.3 Calibration of mass spectrometry data

Methodology. The mass spectrometry quantities were converted to molarity units through a calibration derived MS and NMR measurements of two comparable solutions. Both solutions contained 0.9 M BD and 0.45 M AS initially and were buffered with 0.5 M sodium carbonate to initial pH 5.7, as described in a previous study.[1] MS and NMR measurements of the solutions were taken over two hours of reaction.

MS and NMR measurements were clustered together according to the time they were taken. Five NMR clustered observations were produced with Python's sklearn.cluster library using a K-means approach. MS measurements formed clusters if the time of measurement was close to the mean measurement time of the NMR cluster. As such, there were five clusters that each had MS and NMR data. The mean and standard deviation were reported by the sklearn cluster function for the NMR data and were calculated with the numpy library for the MS data.

It was assumed that the relationship between MS normalized signals (i.e., counts, S_X, normalized to counts PEG-6, S_{PEG6}) was linear with concentration (as measured with NMR). A linear fit was performed between MS normalized signal and NMR concentration measurements, taken from the mean value of each cluster. The MS normalized signal was multiplied by the nominal PEG-6 concentration to account for signal normalization. The ordinary least squares fit was performed with Python's statsmodel package to derive a calibration factor (b) for a species (X) according to the following equation. The reported mean value and standard error were used to derive the best fit and a 95% confidence interval, respectively, of the calibration factor.

$$[X] = b \cdot \frac{S_X}{S_{PEG6}} \cdot [PEG6]$$

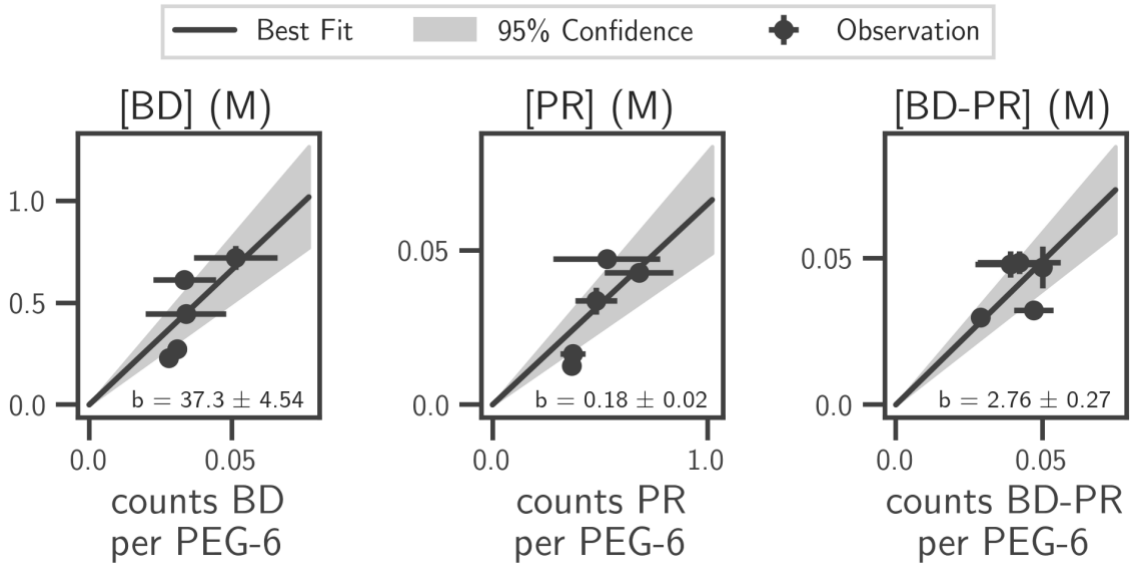

Figure S2-4. Calibration of MS data to concentrations for BD, PR, and BD-PR. Clustered MS and NMR-based observations are shown against the best linear fit and the 95% confidence interval. The calibration factor (b) is shown with its standard error on each panel.

S2-3 Model characterization

S2-3.1 Butenedial first-order lifetime against evaporation

Methodology. Butenedial lifetime against evaporation was estimated as a first order process. According to Maxwellian flux and assuming an ideally mixed particle, the loss of a dissolved species X_i to a gas phase devoid of that species can be described by the following differential equation[3,4]:

$$L_{evap,i} = \frac{d[X_i]}{dt} = -\frac{4\pi r D_{g,i} P_{vap,i}}{kT} \frac{[X_i]}{\sum_i [X_i]}$$

Where r is the particle radius, $D_{g,i}$ is the gas-phase diffusivity of X_i, $P_{vap,i}$ is the saturation vapor pressure of species X_i, k is the Boltzmann constant, T is the gas-phase temperature, and $\sum_i [X_i]$ is the sum of the molarities of all dissolved species. If r and $\sum_i [X_i]$ are approximately constant during evaporation, then the rate law became first order. This is true under humid (>60% RH) conditions with particles that have a largely nonvolatile component (e.g., PEG-6 and/or sulfate). In such a case, the total moles is approximately constant (because the moles of water, the dominant fraction, is more or less constant) as well as solutes that constitute the dominant proportion of particle volume and a major fraction of the molar composition of the particle. The rate law becomes:

$$L_{evap,i} = \frac{d[X_i]}{dt} = -k_{evap}[X_i]$$

The validity of the first order assumption was assessed with butenedial evaporation measurements[3] reproduced below. The particles were composed of 1.6 M butenedial with or without 1.8 M sodium sulfate (and, correspondingly, with 0.9 or 1.9 M PEG-6 as an internal standard). Butenedial first-order lifetime against evaporation was calculated to be 2.6 hours. The plot of the residuals does not show a clear trend, indicating that the first order assumption is valid for butenedial.

The lifetimes were calculated on data by performing a simple ordinary least squares regression on the natural log of the data using the Linear Regression library in Python's sci-kit learn package. Standard errors of the estimated lifetimes were calculated by the library and are provided.

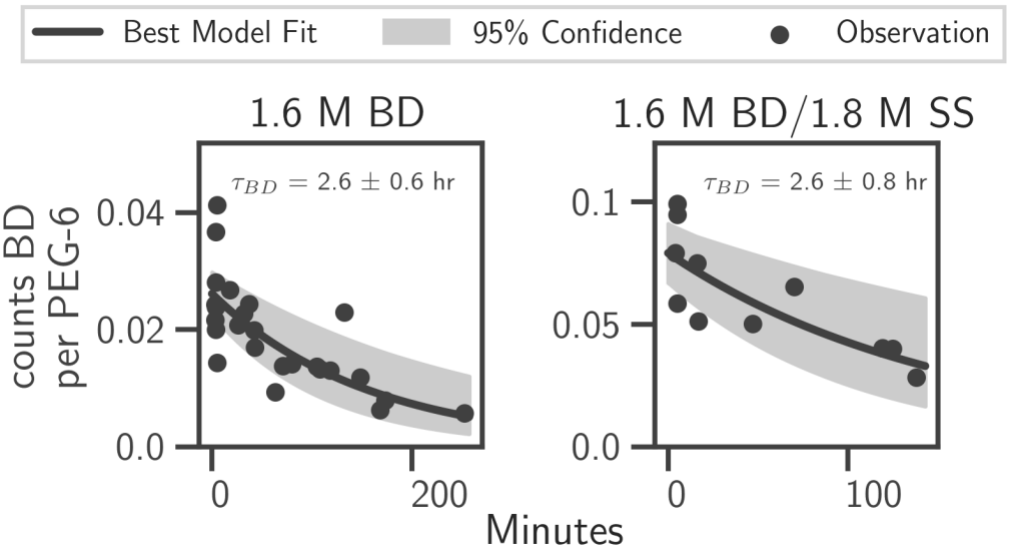

Figure S2-5. Butenedial evaporative loss was observed with and without sodium sulfate (SS). The first order lifetime was computed on measurements of the decay of butenedial signal (normalized to PEG-6) and found to be 2.6 hours, regardless of the SS concentration. The standard error was reported from the fitting and used to derive the 95% confidence window (shaded region) for both plots.

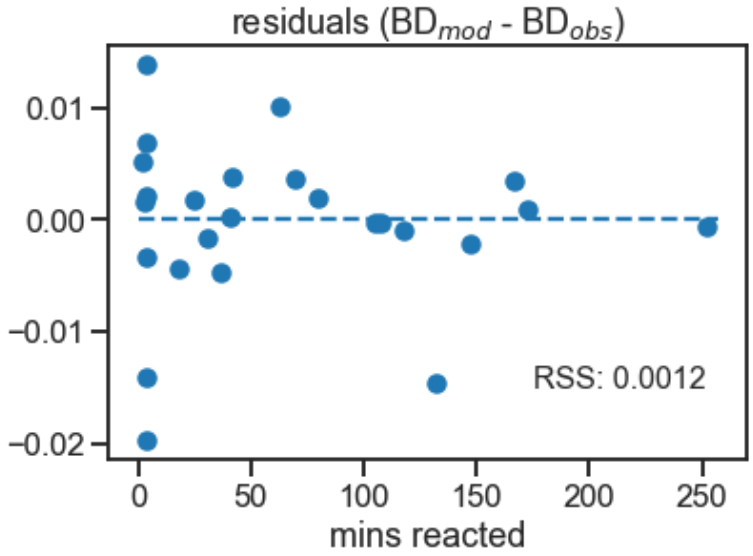

Figure S2-6. Residuals between measured (BD_{obs}) and modeled (BD_{mod}) butenedial normalized signal in butenedial levitated particles without sodium sulfate. Residuals are dispersed without a significant trend around the trendline, with a small residual sum of squares (RSS).

S2-3.2 Loss of butenedial and pyrrolinone from levitated butenedial/AS particles

Methodology. Measurements were also taken in levitated particles produced from "aged" 0.4 M butenedial/0.2 M AS bulk mixtures, defined as bulk mixtures with reaction for over 800 minutes. After around 800 minutes of reaction in bulk liquids, pyrrolinone signal was observed to plateau. Butenedial signal was constant across all reaction timescales in bulk liquids. Therefore, any levitated particles produced from these aged mixtures had a consistent initial butenedial and pyrrolinone signal. "Aged" butenedial/AS levitated particles were produced from these "aged" mixtures and maintained in the electrodynamic balance for several hours to see if butenedial and pyrrolinone were retained in levitated particles.

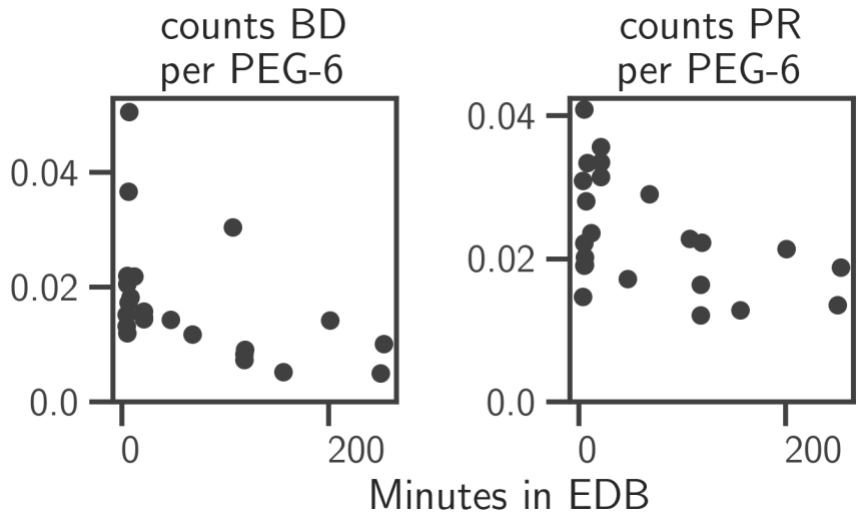

Figure S2-7. Observations of butenedial and pyrrolinone in levitated particles produced from "aged" butenedial/AS bulk mixtures (i.e., time of reaction >800 minutes). Butenedial is still present in particles after 200 minutes of residence in the EDB, and decays at approximately its rate of evaporation. Pyrrolinone has a slower decay rate than butenedial. It is therefore shown that pyrrolinone or butenedial loss does not prevent reaction from being observed in levitated butenedial/AS particles.

S2-3.3 Calculation of NH_3

Table S2-2. Calculated values in butenedial particle + NH_3(g) experiments.

NH_3(aq), mM	C_{NH3}, ppm	NH_3(p), mM
0.05	0.7	0.04
0.29	3.5	0.22
1.5	18	1.1
15	180	11

The bubbler was filled with aqueous ammonia solutions with known NH_3(aq). Using Henry's Law and assuming that the ammonia vapor pressure was at the same % saturation as water (i.e., $C_{NH3} = RH \times C_{NH3,sat}$), the gas-phase NH_3 mixing ratio (C_{NH3}) was calculated.

$$C_{NH_3} = RH \times \frac{NH_3(aq)}{H}$$

Where H is the Henry's Law constant for ammonia (61 M atm^{-1}).[5] The particle-phase concentration of ammonia (NH_3(p)) was also calculated with Henry's Law from the gas-phase NH_3, which simplifies to the following equation.

$$NH_3(p) = RH \times NH_3(aq)$$

S2-3.4 Model sensitivity to NH_3 and pH

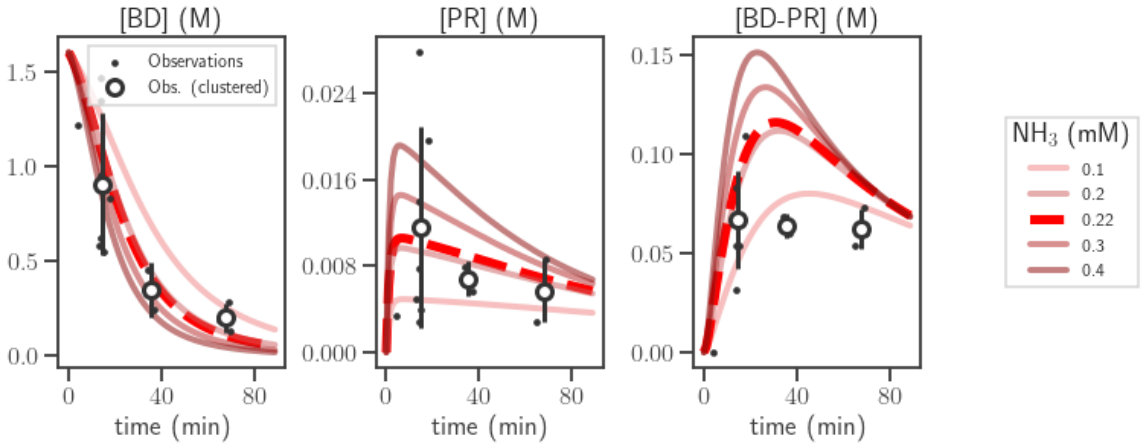

Figure S2-8. Comparison of observed and modeled butenedial (BD), pyrrolinone (PR), and butenedial-pyrrolinone dimer (BD-PR) concentrations in levitated butenedial particles exposed to humidified N_2 gas with 3.5 ppm NH_3. Measurements of each species are calibrated and are shown as particulate concentrations. The model is run at pH 6.9, the best fit determined through a least-squares analysis, and 1.6 M initial butenedial. Particle NH_3 was 0.1, 0.2, 0.22, 0.3, and 0.4 mM in model runs, as shown.

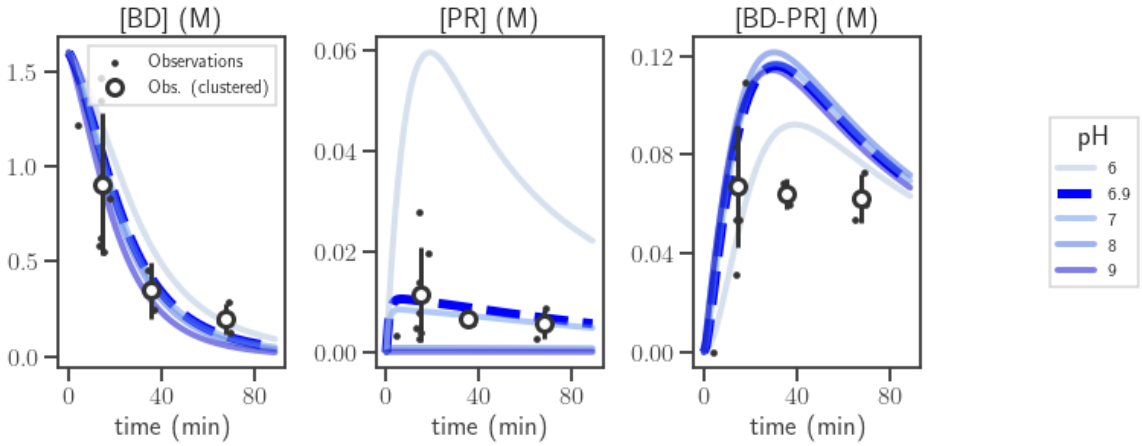

Figure S2-9. Comparison of observed and modeled butenedial (BD), pyrrolinone (PR), and butenedial-pyrrolinone dimer (BD-PR) concentrations in levitated butenedial particles exposed to humidified N_2 gas with 3.5 ppm NH_3. Measurements of each species are calibrated and are shown as particulate concentrations. The model is run at 0.22 mM NH_3 (the equivalent concentration of particles equilibrated with 3.5 ppm NH_3), and 1.6 M initial butenedial. Particle pH was 6, 6.9, 7, 8, or 9 in model runs, as shown. PR is the species that is most sensitive to particle pH, although agreement is strongest near pH 6.9. Butenedial is not found to be sensitive to pH.

S2-3 References

(1) Hensley, J. C.; Birdsall, A. W.; Valtierra, G.; Cox, J. L.; Keutsch, F. N. Revisiting the Reaction of Dicarbonyls in Aerosol Proxy Solutions Containing Ammonia: The Case of Butenedial. *Atmos. Chem. Phys.* **2021**, *21* (11), 8809–8821. https://doi.org/10.5194/acp-21-8809-2021.

(2) Birdsall, A. W.; Krieger, U. K.; Keutsch, F. N. Electrodynamic Balance–Mass Spectrometry of Single Particles as a New Platform for Atmospheric Chemistry Research. *Atmos. Meas. Tech.* **2018**, *11* (1), 33–47. https://doi.org/10.5194/amt-11-33-2018.

(3) Birdsall, A. W.; Hensley, J. C.; Kotowitz, P. S.; Huisman, A. J.; Keutsch, F. N. Single-Particle Experiments Measuring Humidity and Inorganic Salt Effects on Gas-Particle Partitioning of Butenedial. *Atmos. Chem. Phys.* **2019**, *19* (22), 14195–14209. https://doi.org/10.5194/acp-19-14195-2019.

(4) Seinfeld, J. H.; Pandis, S. N. *Atmospheric Chemistry and Physics: From Air Pollution to Climate Change*; John Wiley & Sons, Incorporated: New York, 2016.

(5) Sander, R. Compilation of Henry's Law Constants (Version 4.0) for Water as Solvent. *Atmos. Chem. Phys.* **2015**, *15* (8), 4399–4981. https://doi.org/10.5194/acp-15-4399-2015.